EARTHQUAKE ENGINEERING AND STRUCTURAL DYNAMICS
*Earthquake Engng Struct. Dyn.* 2009; **38**:587–607
Published online 13 February 2009 in Wiley InterScience (www.interscience.wiley.com). DOI: 10.1002/eqe.897

# Simulation of the shaking table test of a seven-story shear wall building

Paolo Martinelli[1,*,†,‡] and Filip C. Filippou[2,§]

[1]*Department of Structural Engineering, Politecnico di Milano, P.za L. da Vinci 32, 20133 Milano, Italy*
[2]*Department of Civil and Environmental Engineering, University of California, Berkeley, Davis Hall, CA 94720, U.S.A.*

## SUMMARY

This paper presents the simulation of the nonlinear dynamic response of a full-scale seven-story reinforced concrete shear wall shaking table specimen under base excitations representing four earthquake records of increasing intensity. The study was motivated by the participation in the blind prediction contest of the shaking table specimen organized by University of California at San Diego (UCSD), NEES, and Portland Cement Association (PCA). Owing to the time constraints of the contest a relatively simple two-dimensional (2d) model was used for the shear wall specimen. In this model, the shear wall was represented by 2d beam–column elements with fiber discretization of the cross-section that account for the interaction of the axial force with the bending moment. Upon conclusion of the contest, the available experimental measurements permitted a thorough examination of the analytical results. While the measured data confirmed the excellent accuracy of the model predictions, some limitations also became apparent. The paper addresses the benefits and limitations of the selected modeling strategy and investigates the sensitivity of this type of model to parameter selection. Copyright © 2009 John Wiley & Sons, Ltd.

Received 28 May 2008; Revised 26 October 2008; Accepted 5 January 2009

KEY WORDS: R/C shear wall; fiber beam–column element; shaking table

*Correspondence to: Paolo Martinelli, Department of Structural Engineering, Politecnico di Milano, P.za L. da Vinci 32, 20133 Milano, Italy.
†E-mail: pmartinelli@stru.polimi.it
‡Research Associate.
§Professor.

Contract/grant sponsor: NEESinc
Contract/grant sponsor: Portland Cement Association
Contract/grant sponsor: University of California at San Diego
Contract/grant sponsor: Department of Structural Engineering of the Politecnico di Milano

## 1. INTRODUCTION

Reinforced concrete (R/C) shear walls are commonly used as the lateral load-resisting system of structures in zones of high seismic risk. In medium- to high-rise R/C buildings, well-designed and detailed R/C shear walls provide the necessary strength, stiffness, and deformation ductility to ensure the satisfactory performance of the structure in the service, damage and ultimate limit states.

With increasing attention to damage limit states following the extensive damage caused by recent strong earthquakes (Northridge, 1994; Kobe, 1995; Kocaeli, 1999; Chi-Chi, 1999), performance-based design guidelines favor the use of shear walls either as single elements (that are coupled with moment-resisting frames), or in the form of T, U, and L-shaped open or tubular cross-sections. Within the framework of modern performance-based design codes, the need for a more accurate seismic response assessment of these structures in the form of nonlinear static analysis, or, nonlinear time-history analysis brings to the fore the issue of suitable shear wall models for nonlinear static and dynamic analysis. In this regard, two approaches are common in structural engineering practice: (a) the first involves the plane-stress finite element models, and (b) the second involves the use of beam–column elements. The first approach is quite common under linear elastic response conditions, but is not economic under nonlinear conditions, particularly, since no robust and reliable constitutive models of R/C are available. Beyond the complexity of the model, the time requirement for the post-processing and interpretation of the analytical results makes such models forbiddingly expensive for the evaluation of ordinary structures. The second approach is economic, particularly, since beam–column elements are now widely available in commercial software packages, and the results can be readily post-processed and interpreted. Since the nonlinear behavior of most well-designed and detailed shear walls with an aspect ratio greater than 3 is dominated by flexure, it is expected that the simplicity of the element does not sacrifice accuracy in this case. It is the purpose of this study to address this issue with reference to the nonlinear dynamic response of a slender, well-designed and detailed shaking table shear wall specimen under a sequence of strong base excitations representing four recorded earthquake ground motions of increasing intensity up to a maximum acceleration of $0.93g$.

The study was motivated by the participation in a blind prediction contest for the simulation of the response of a full-scale vertical slice of a seven story R/C shear wall building that was organized by the School of Engineering at the University of California at San Diego (UCSD), the Portland Cement Association (PCA), and the NEES Consortium. The organizers provided the participants with the relevant material and geometric properties of the wall and the input base excitation records, but kept the experimental results secret. Approximately two months were available for the conduct of the analytical studies, the interpretation of the response, and the submission of the results. An important objective of the contest was the comparative evaluation of different modeling strategies, and the identification of their benefits and limitations under blind prediction conditions. Furthermore, the organizers' intent was to identify model uncertainties and problems in parameter selection to study the model sensitivity to parameter selection, and to establish the reliability and robustness of different modeling strategies for use in professional practice. Finally, the contest was supposed to identify the practical needs for the improved simulation capabilities, and showcase the benefits and assess the future needs of large-scale testing.

The paper describes the development of the analytical model, the blind prediction of the dynamic response for the contest, and the critical appraisal and improvement of the model following the publication of the measured data upon conclusion of the contest.



DOI: 10.1002/eqe

## 2. DESCRIPTION OF THE R/C SHEAR WALL SPECIMEN

### *2.1. Geometry and mass distribution*

The test specimen is a seven-story full-scale R/C shear wall structure (Figure 1) [1–4]. The structure was designed with the displacement-based capacity approach for a site in Los Angeles [5, 6]. This resulted in designing lateral forces that are smaller than those currently specified in U.S. building codes for regions of high seismic risk. The total height of the specimen is 19.96 m and the total mass is $226 \times 10^3$ kg. The building is the tallest structure ever tested on a shaking table. The specimen is made up of a 3.65 m wide web wall and two transverse structural elements: a 4.88 m wide flange wall and a precast segmental pier column. The web and the flange walls are fixed at the base. The web wall provides lateral resistance in the direction of loading, while the other two structural elements provide transverse and torsional resistance to the test structure. The thickness of the web wall is 203 mm at the first and seventh floor and 152 mm elsewhere. The thickness of the flange wall is 203 mm at the first floor and 152 mm elsewhere. The foundation and the floor plan view of the specimen are shown in Figure 2. The direction of the input ground motion is parallel to the web wall, as depicted with a double-headed arrow in the plan view of Figure 2.

The $3.65\,\text{m} \times 8.13\,\text{m}$ simply supported slab of each floor rests on the walls and on auxiliary gravity columns, as shown in Figure 2. At each floor, the flange wall is connected to the slab and to the web wall through a slotted connection. A detail of this connection is shown in Figure 3. The segmental pier column is connected to the slab through a pin–pin horizontal steel truss. The pier was pinned at the base in the east–west (E–W) direction and fixed in the north–south (N–S) direction. For the gravity columns, high-strength steel pin–pin rods grouted in 102 mm pipes were used.

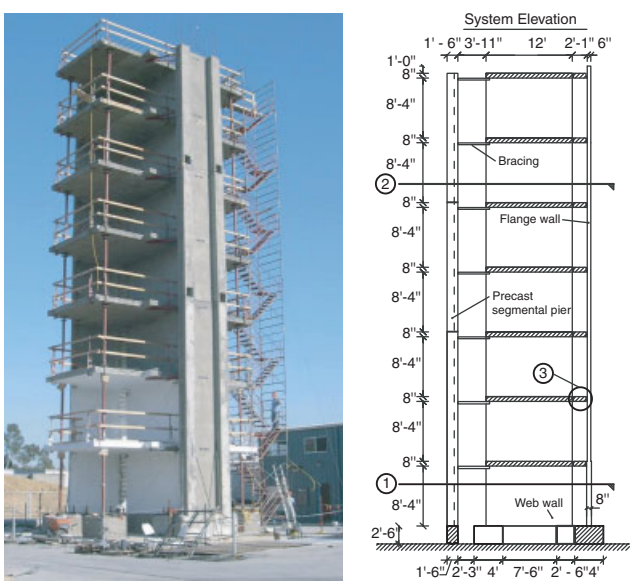


Figure 1. View and elevation of NEES–UCSD specimen (U.S. customary units).



DOI: 10.1002/eqe

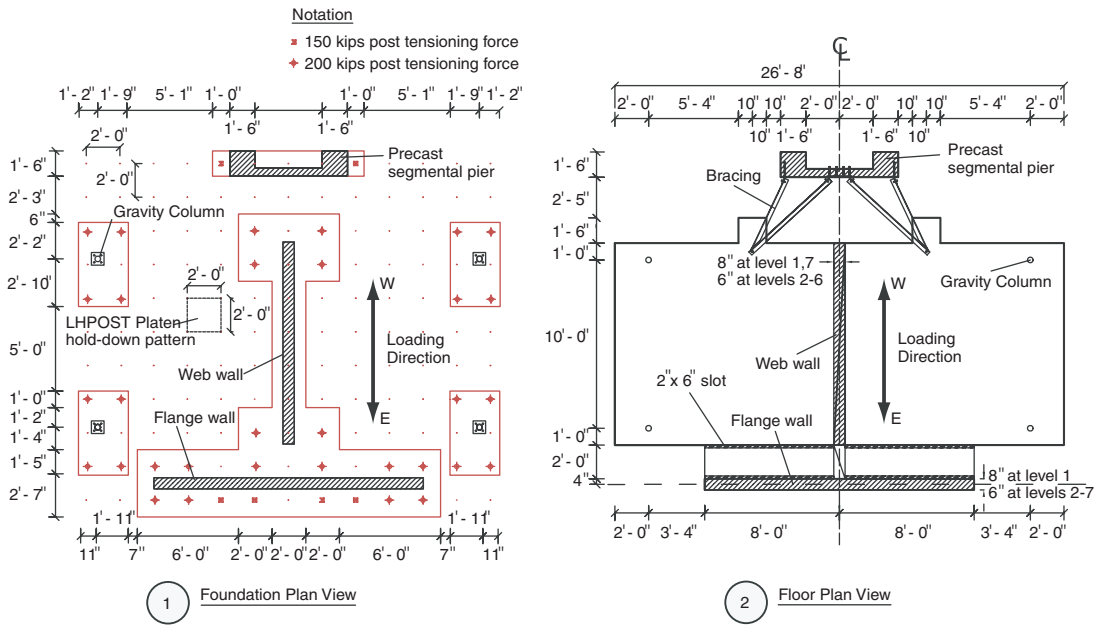


Figure 2. Foundation and typical floor plan of the specimen (U.S. customary units).

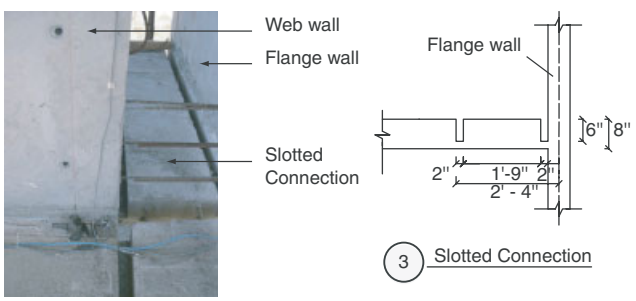


Figure 3. View and particular of the slotted connection (U.S. customary units).

### 2.2. *Material properties*

Tunnel steel forms were used for the construction of the walls and slabs. The concrete had a compressive cylinder strength of 28 MPa and an average elastic modulus of 29 GPa, while the steel was A615 grade 60. The construction sequence involved casting a level of the web and flange walls together with the slab. The segmental pier column was precast in three pieces and assembled afterwards using mortar bed joint and post tensioning.

The reinforcement details of the web and the flange wall are shown in Figure 4. The reinforcement of the web wall in the first and seventh story consisted of two layers of vertical reinforcement (8#5) and confinement mesh (#3@4 in Baugrid) at each end with a single layer of reinforcement (13#4@10 in) in between. The reinforcement of the other stories consisted of a single layer of



DOI: 10.1002/eqe

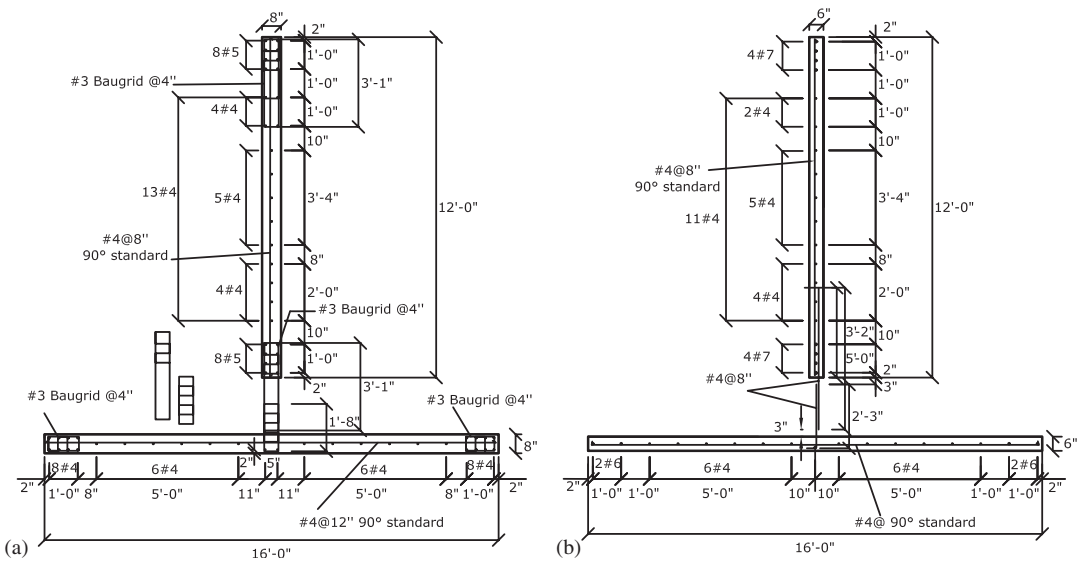


Figure 4. Reinforcement details for the wall specimen: (a) first level and (b) levels 2–6 (U.S. customary units).

vertical reinforcement with 4#7 at each end and 11#4@10 in in between. No confinement reinforcement was provided in the stories two through six. A single layer of horizontal reinforcement (#4@8 in) was provided over the entire wall height. The resulting longitudinal reinforcing ratio is $\rho_l = 0.66\%$ at the first and seventh story and $\rho_l = 0.81\%$ elsewhere.

The reinforcement of the first story was anchored to the foundation and extended until the soffit of the first floor slab. In the other stories, the reinforcement of the lower story was lap spliced with the reinforcement of the upper story. Additional transverse reinforcement was used at the lap splice location in the stories two–six. A capacity-based design was followed for the design of the lap splice region. The total steel reinforcement area of the lap splice was equal to the reinforcement area of the lower story and exceeded slightly the reinforcement area of the upper story.

### *2.3. Instrumentation*

The motion of the shaking table and the global and local behavior of the specimen were monitored through a dense network of instrumentation of 139 accelerometers, 58 displacement transducers, 28 string potentiometers, 314 strain gages and 23 pressure transducers. A videogrammetric system and an array of 50 Hz GPS devices with a resolution of 3 mm were used to measure the displacements. Since the inelastic deformations were expected to concentrate at the lower stories, a denser network of displacement transducers and string potentiometers were deployed at those locations. In total, the dynamic response of the structure including the motion of the shaking table and the response of the reaction block with the surrounding soil were monitored for more than 600 devices during the test.

A dense network of longitudinal, transverse, and vertical accelerometers was also deployed. These accelerometers were placed on each slab, at each mid-story location of the web wall, and



DOI: 10.1002/eqe

at the top of the post tensioned pier and of the flange wall. Finally, 16 accelerometers were placed at the foundation and at the shaking table platen.

The story shear force was determined from the product of the floor mass with the corresponding recorded absolute horizontal acceleration. The latter was obtained from the floor slab accelerometer, closest to the centroid of the web wall section. The layout of accelerometers on the floor slab is given by Panagiotou *et al.* [2].

### *2.4. Test program*

The experimental program subjected the specimen to different levels of excitation. The input motion consisted of four accelerograms and was applied in the direction parallel to the web wall, i.e. in the E–W direction in Figure 2. The four input motions are denoted with EQ1, EQ2, EQ3, and EQ4, respectively. The first two records are the longitudinal and transverse component of the 1971 San Fernando earthquake record at the Van Nuys station. The third record is the longitudinal component of the 1994 Northridge earthquake record at the Oxnard Boulevard station in Woodland Hill. The last record is the Sylmar Olive View Medical Center 360° component from the same earthquake. The test program also included a low-intensity white noise excitation in-between the earthquake tests. The response spectra of the first three earthquake records are slightly higher than the site response spectrum for 50% probability of exceedance in 50 years. The large intensity earthquake record has a spectral acceleration in the period range of interest above the site response spectrum for 10% probability of exceedance in 50 years. The acceleration and displacement response spectra for 5% damping of the signal recorded on the tables during the tests are given in Figure 5. The fundamental period of the specimen at the beginning of the test program is indicated with a dashed line. For the white noise tests $2\%g$, $3\%g$ and $5\%g$ root mean square (RMS) motions were used. Ambient and white noise vibrations were measured with accelerometers and linear variable differential transformers (LVDTs). These were used for the system and damage identification before and after every earthquake test, thus helping to establish the degree of damage after each input motion. During the high-intensity motion, the structure experienced significant damage at its base.

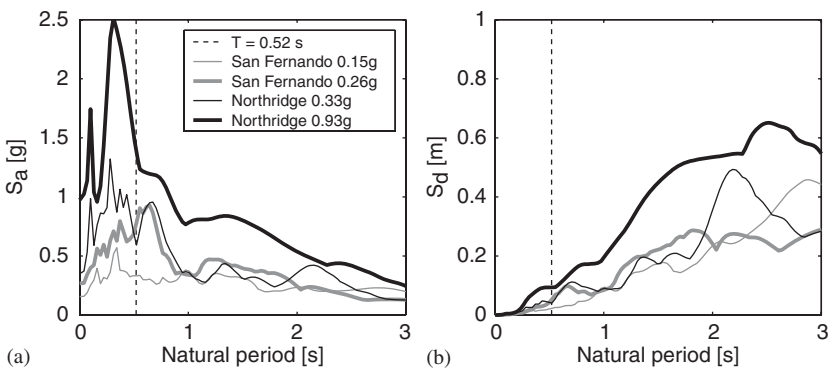


Figure 5. (a) Acceleration and (b) displacement response spectra for 5% damping.



DOI: 10.1002/eqe

## 3. SPECIMEN MODEL

### *3.1. Selection of simulation platform*

The platform selected for the seismic response simulation is OpenSees [7], an open-source software framework with an extensive library of finite elements for the earthquake engineering analysis of structural and geotechnical systems. In contrast to most commercial software with traditional design, the open source modular architecture of OpenSees permits the easy customization of material and element models, and solution strategies. Moreover, post-processing scripts can automate the process of response evaluation. The selection of the software platform was conditioned by the available structural elements and by the familiarity of the research team with its procedures.

With respect to the present study, OpenSees offers capabilities for modal analysis of linear elastic response and for nonlinear dynamic time-history analysis with uniform or multi-support excitation. Either the Newmark method or the HHT method is available for time integration. Finally, any local or global response variable can be monitored during the analysis with the use of recorder objects.

Because of the lack of a special purpose shear wall element in the OpenSees element library and the relative slenderness of the shear wall specimen, it was decided to use a beam–column element to represent the response of the shear wall. Shear effects were not expected to be significant for this well-designed slender wall. This assumption was subsequently vindicated by the experimental results that evidenced almost exclusively flexural cracking at the base of the wall.

### *3.2. Shear wall element*

Several types of beam–column elements are available in OpenSees: a distributed inelasticity finite element with several integration points along the span allowing for inelastic deformations to take place at any one of these points, a plastic zone element in which inelastic deformations take place at the ends of the element [8], and an aggregate element of a linear elastic beam–column with inelastic springs at the element ends. Most of these elements are based on the force formulation that interpolates the internal element forces from the basic element forces, thus satisfying exactly the element equilibrium under linear kinematics. The distributed inelasticity element is also available in the displacement formulation, in which the element displacement field is expressed as a function of the nodal displacements [9].

In this work, the distributed inelasticity beam–column element with force formulation is selected [10]. The section response is derived from the integration through the depth of the inelastic material response, a formulation that is known under the name of fiber section. For this reason, this element will be hereafter referred to as fiber beam–column element.

The decision to select this element and section description stems from the validation of this element in previous correlation studies, its numerical robustness, and its computational efficiency. The fiber discretization of the cross-section allows for the interaction of the axial force and bending moment to be rationally accounted for. Last but not least, the fiber beam–column element was ideal to meet the short time frame of the blind prediction contest, because of its ability to represent the hysteretic response of an R/C member with a single element. This fact played an important role in keeping the simulation times short allowing for many seismic response analyses to be conducted so as to test the parameter sensitivity of the shaking table models.

In the force-based fiber beam–column element of OpenSees, the element force–deformation behavior is described in a basic reference system that does not include the rigid body modes. The transformation of these response quantities to the global reference system can be done for linear



DOI: 10.1002/eqe

geometry or nonlinear large displacement geometry through the corotational formulation [11]. This approach uncouples the nonlinear geometry of frame elements from the nonlinear material response. The nonlinear geometric transformations are implemented once for all frame elements and are readily available. Thus, the focus of the analyst is on the representation of the nonlinear material response in the basic reference system.

The constitutive behavior of the element can be described either by integration of appropriate nonlinear material constitutive relations over the cross-section of the element or by postulating a constitutive relation for section force–deformation resultants. The latter approach typically requires careful validation and is known to work well only for elastic–perfectly plastic material response. It is, therefore, not pursued further in this study.

Under the assumption of a Bernoulli beam that the plane sections remain plane after deformation, uniaxial laws suffice for the description of the constituent materials of an R/C member with a fiber discretization of the cross-section. This modeling approach describes quite well the shift of the neutral axis across the wall section during the inelastic response of the element. Earlier correlation studies have shown that this approach is very suitable for representing the hysteretic behavior of an R/C member under constant or variable axial force.

For the concrete fibers (or layers in a 2d model), the modified Kent–Park model was used for the response in compression [12, 13]. It consists of an ascending parabolic branch and a descending linear part for strains greater than the strain corresponding at peak stress. The parameter $\kappa$ (Figure 6(a)) is a coefficient that accounts for the volumetric confinement ratio and is equal to 1 for unconfined concrete. The parameter $Z_m$ (Figure 6(a)) defines the strain softening slope and depends on the coefficient $\kappa$ [13, 14]. To simulate the behavior in tension and the tension stiffening effect, a linear elastic branch is followed by a linear softening branch up to zero stress in tension (Figure 6(b)). The steel fibers follow the nonlinear model of [15], as modified by Filippou *et al*. [16] to include isotropic-hardening effects (Figure 6(c)). The mathematical relation describes a transition curve from an asymptote having slope $E_0$ (Young's modulus) to another asymptote of slope $E_1 = bE_0$; the parameter $b$ denotes the strain-hardening ratio of the second asymptote with respect to the first one and parameter $R_0$ controls the curvature of the transition from the elastic to the plastic-hardening branch. The evolution of this parameter with cyclic strain history describes the Bauschinger effect.

### *3.3. Model for shaking table specimen*

The limited time frame of the 'blind contest' and the 2d excitation in the plane of symmetry led to the selection of a 2d model for the shaking table specimen with a lumped mass at each floor. This model did not account for the 3d effects of deformation compatibility between the web wall, the slab, and the flange wall. These effects played a role in the prediction of the internal force distribution of the web wall, but did not compromise appreciably the accuracy of displacement and deformation values as it will be shown in the following sections. The model uses one nonlinear fiber beam–column element at the centerline of the web wall and one at the centerline of the flange wall for each story of the specimen. The number of integration points for a force-based element should be selected with the following criteria in mind: (a) in the absence of distributed element loading three (3) to four (4) integration points suffice for accuracy, (b) the plastic hinge length is equivalent to the weight of the integration point nearest to the end, if inelastic deformations concentrate at the element ends, as is the case in frame and shear wall structures under earthquake loading, (c) with a small number of integration points localization issues do not arise, because member subdivision



DOI: 10.1002/eqe

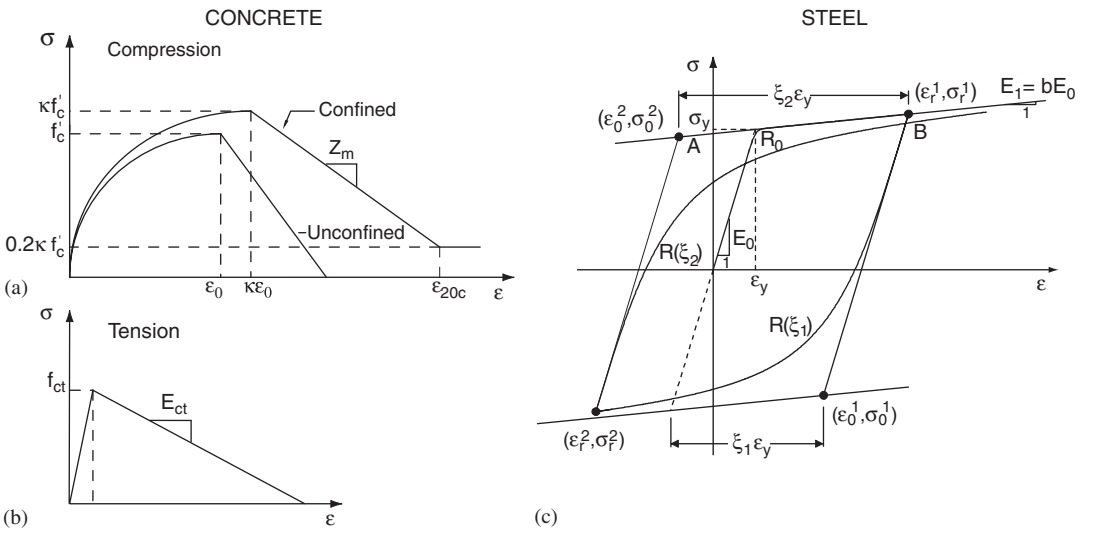


Figure 6. Constitutive material models: (a) concrete in compression; (b) concrete in tension; and (c) steel.

to several elements is not required for accuracy in the force-based beam–column element. In view of these considerations, three integration points were used for each beam–column element of the shear wall specimen model. Figure 7 provides an overview of the nodes and elements layout of the model.

The footings under the web and the flange wall were very large and were longitudinally prestressed so as to remain elastic during the test. Thus, a single linear elastic element was used under each wall. The properties of these linear elements were based on the gross section with a Young modulus of concrete of $E_c = 27\,500$ MPa close to the average measured value.

The sole purpose of the precast column element was the torsional stability of the specimen that was achieved with braces to the slab. The precast column and the braces were designed to remain elastic during the tests. In the model the precast column element was represented with a linear elastic frame element and the braces with linear elastic truss elements. The elastic properties were based on the dimensions of these members and the reported material properties. Rigid end offsets were used to connect the web wall centerline with the truss element representing the slotted connection between the flange wall and the web wall. The axial rigidity $EA = 18.4 \times 10^6$ kN of this connection is high enough to ensure that the horizontal displacement of the web and the flange wall are equal at each floor. The small bending moment and shear force per unit of length that can be transferred by the slotted connection between the flange and web wall was therefore neglected.

The web wall cross-section in stories 1 and 7 was subdivided into 56 concrete layers with the outermost six layers having one-third the area of the remaining layers. The web wall cross-section in stories 2–6 was subdivided into 44 concrete layers. The analytical model distinguishes two zones of concrete material behavior: the outer layers of the cross-section in stories 1 and 7 were assumed as confined by the presence of transverse reinforcement, while the remaining layers of the cross-section in stories 1 and 7 and the entire section in stories 2–6 were assumed as unconfined. The material properties for the unconfined concrete were based on the measured values of zone 'c3' in the first story of the web wall from the experimental study [1]. Table I lists the material



DOI: 10.1002/eqe

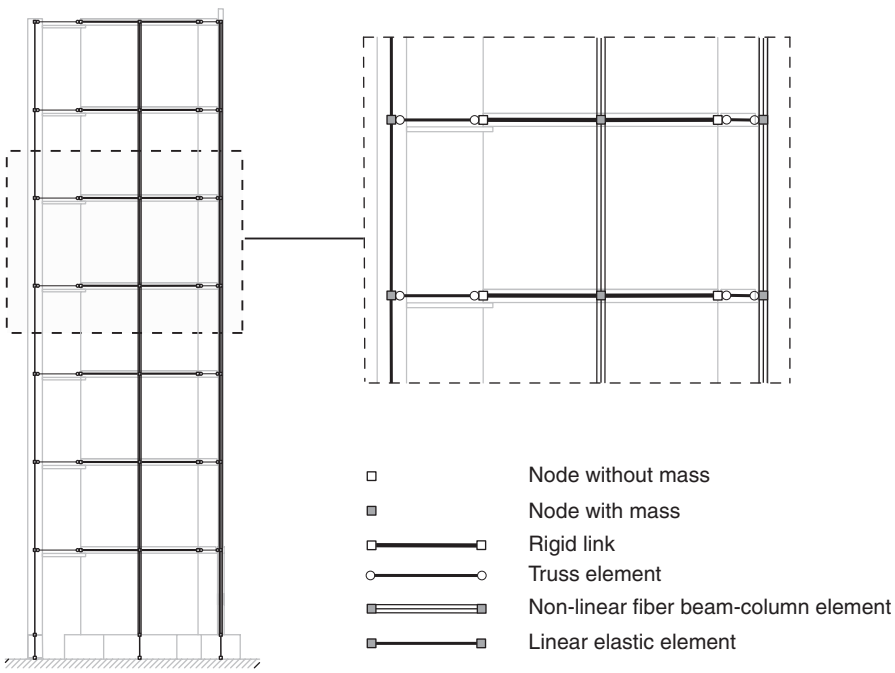


Figure 7. Numerical model of the shear wall specimen.

Table I. Concrete material properties assumed in the analyses.

| Concrete Type | $f'_c$ (MPa) | $\varepsilon_0$ $\times 10^{-3}$ | $\varepsilon_u$ $\times 10^{-3}$ | $\kappa$ | $Z_m$ | $f_{ct}$ (MPa) | $E_{ct}$ (MPa) |
|---|---|---|---|---|---|---|---|
| Unconfined | −37.9 | −2.70 | −5.09 | 1 | 376 | 3.8 | 2800 |
| Confined | −45.8 | −3.26 | −30.3 | 1.21 | 30 | 3.8 | 2800 |

properties for the two types of concrete used in the simulation studies. For simplicity, a single value of 450 MPa was used for the yield strength of the reinforcing steel in the analytical model. This value is close to the average of measured values from the coupon tests of the specimen.

The final model used for the blind prediction contest evolved over the course of several weeks by studying the effect of components on the fundamental frequency. The model development started with the consideration of the web wall only with the mass of the specimen assumed lumped at each floor, including also the mass of the slab. This model resulted in a first natural frequency of 2.29 Hz, as compared with the value of 1.91 Hz that was obtained from acceleration measurements under ambient vibration. The model was then modified to include the flange wall and the slotted connections between the web and the flange wall were introduced as rigid links. This model turned out to be very stiff with a first natural frequency of 4.17 Hz. After releasing the moment transfer capability of the slotted connections and allowing for the axial force transfer only, the first natural frequency of the model decreased to 2.06 Hz. This model was then modified with the inclusion



DOI: 10.1002/eqe

Table II. Experimental and analytical natural frequencies.

| | Experimental frequencies (Hz) | Nonlinear model (Hz) |
|---|---|---|
| 1st L-mode | 1.91 | 2.05 |
| 1st L–T mode | 6.99 | — |
| 2nd L-mode | 10.84 | 12.21 |
| 3rd L-mode | 23.39 | 19.8 |

of the post tensioned pier resulting in a slight reduction of the first natural frequency to 1.95 Hz. Finally, the inclusion of the rotary inertia of the floor mass resulted in a slight reduction of the first natural frequency of the model to 1.94 Hz. Since this value was very close to the measured first frequency of the shaking table specimen, no further modifications were introduced, and the last model served as the starting point for the nonlinear response simulations.

The replacement of the linear elastic with the nonlinear beam–column element for the web and the flange wall of the specimen required a re-evaluation of the initial frequency, which now depends on the initial material moduli of reinforcing steel and concrete in the fiber model of the cross-section. In this regard it was assumed that the wall section is under sufficient compression due to gravity for the initial modulus of concrete to be the tangent modulus in compression. With this assumption the initial frequency of the model with the fiber beam–column elements for the web and flange wall was equal to 2.05 Hz, slightly higher than for the linear elastic elements. The first three longitudinal (L) natural frequencies of the shaking table specimen from ambient vibration data of the undamaged state are compared with the frequencies of the model in Table II. The first experimentally measured coupled longitudinal–torsional (L–T) frequency is also reported. These experimental data were available only after the competition [17].

## 4. SIMULATION OF THE SHAKING TABLE SPECIMEN RESPONSE

The numerical results presented in this paper fall into two categories: (a) results obtained for the initial submission to the 'blind' contest without the knowledge of the measured response and (b) results obtained from refinements of the model after the competition in an attempt to match better the measured response. The former are reported in Section 4.1 and the latter are reported separately in Section 4.2. The post-contest results were obtained without drastic changes to the original model, as such modifications were not warranted by the quality of the original predictions. Moreover, the lack of funding did not allow for an extensive post-contest study. Nonetheless, the post-contest results benefited from the availability of the experimental results and from the insight gained from the results of other blind prediction participants in a workshop at the conclusion of the contest [18].

The gravity loads were applied first in a static analysis, followed by the dynamic analysis of the model. The dynamic analyses of the specimen were conducted with a single continuous sequence of concatenated acceleration records from EQ1 to EQ4. All nonlinear time-history analyses adopted the Newmark time integration method of constant acceleration ($\beta = 0.25, \gamma = 0.5$), with a time step equal to $\Delta t = 0.01$ s. Rayleigh damping was assumed with the damping matrix proportional to the mass and initial stiffness matrix. The constants were calibrated to give a damping ratio of 1.0%



DOI: 10.1002/eqe

for the first two flexural modes of the specimen in the plane of excitation. This is a reasonable assumption in view of the experience from field testing of structures that shows the measured damping ratios of less than 2% in the elastic range [19]. The same viscous damping matrix was used for all base motions. The Newton–Raphson iteration method was used to satisfy the equations of motion in each time step. The convergence of the algorithm was based on the relative work increment. If a time step failed to converge, it became necessary to switch to a modified Newton method with constant stiffness equal to the initial stiffness of the time step. This resulted in a large number of iterations, but this measure was used rather sparsely.

### *4.1. Blind prediction evaluation of the shear-wall specimen*

The assessment of the quality of the numerical prediction of the response is based on the envelope of the maximum values for floor lateral displacement, interstory drift, residual lateral displacement, horizontal floor acceleration, story shear force, and overturning moment, which were required for the competition. These quantities are depicted in Figure 8(a)–(f), with a solid line representing the experimental values and a dashed line representing the numerical results; different markers are used for each input motion.

The agreement between measured and predicted displacement and the interstory drift values in Figure 8(a)–(b) is very good for EQ1 and EQ4 and quite good for EQ2 and EQ3. The increasing deformation caused by the increasing intensity of the input motions is apparent in the envelope values. The measured and the predicted displacement and the interstory drift envelopes indicate the highly inelastic response of the specimen during EQ4 with the formation of a plastic hinge at the base of the web wall. Further support of this fact is provided by the permanent inelastic deformations of the analytical model after the last input motion, in good agreement with measured values (Figure 8(c)). The agreement between measured and predicted floor acceleration values is also more than satisfactory (Figure 8(d)).

The experimental shear force and the overturning moment were evaluated at the centerline of the web wall and took into account the inertial effects of all elements of the structure. The reported story shear values in Figure 8(e) are based on the static restoring forces of all elements and do not account for the damping force contribution. These are compared with the experimental values, which are determined from the product of the story mass with the measured horizontal floor acceleration, and thus include the damping force contribution. In addition to the damping force discrepancy between measured and analytical story shear and the overturning moment values, the observed underestimation of the measured values is also due to the exclusion of the effect of the slab and of the moment transfer of the slotted connection in the model. These effects give rise to an additional axial force in the web wall of the specimen that affects the moment capacity and, thus, the static restoring force value. These response aspects will be discussed in more detail in the next section.

For each input motion the maximum analytical time-history values are compared with the experimental values for top horizontal displacement ($u_{\text{top}}$), top interstory drift ($\text{drift}_{\text{top}}$), top residual displacement ($u_{\text{top,res}}$), top horizontal absolute acceleration ($a_{\text{top}}$), base overturning moment ($M_{\text{base}}$), and base shear force ($V_{\text{base}}$) in Table III. The percentage errors reported in Table III permit a quick assessment of the accuracy of the analytical predictions. It is noteworthy that the agreement for the top floor displacement, drift and acceleration is in general better than the agreement for the base shear and overturning moment. As will be discussed subsequently, the agreement between the analytical values for base shear and overturning moment was significantly



DOI: 10.1002/eqe

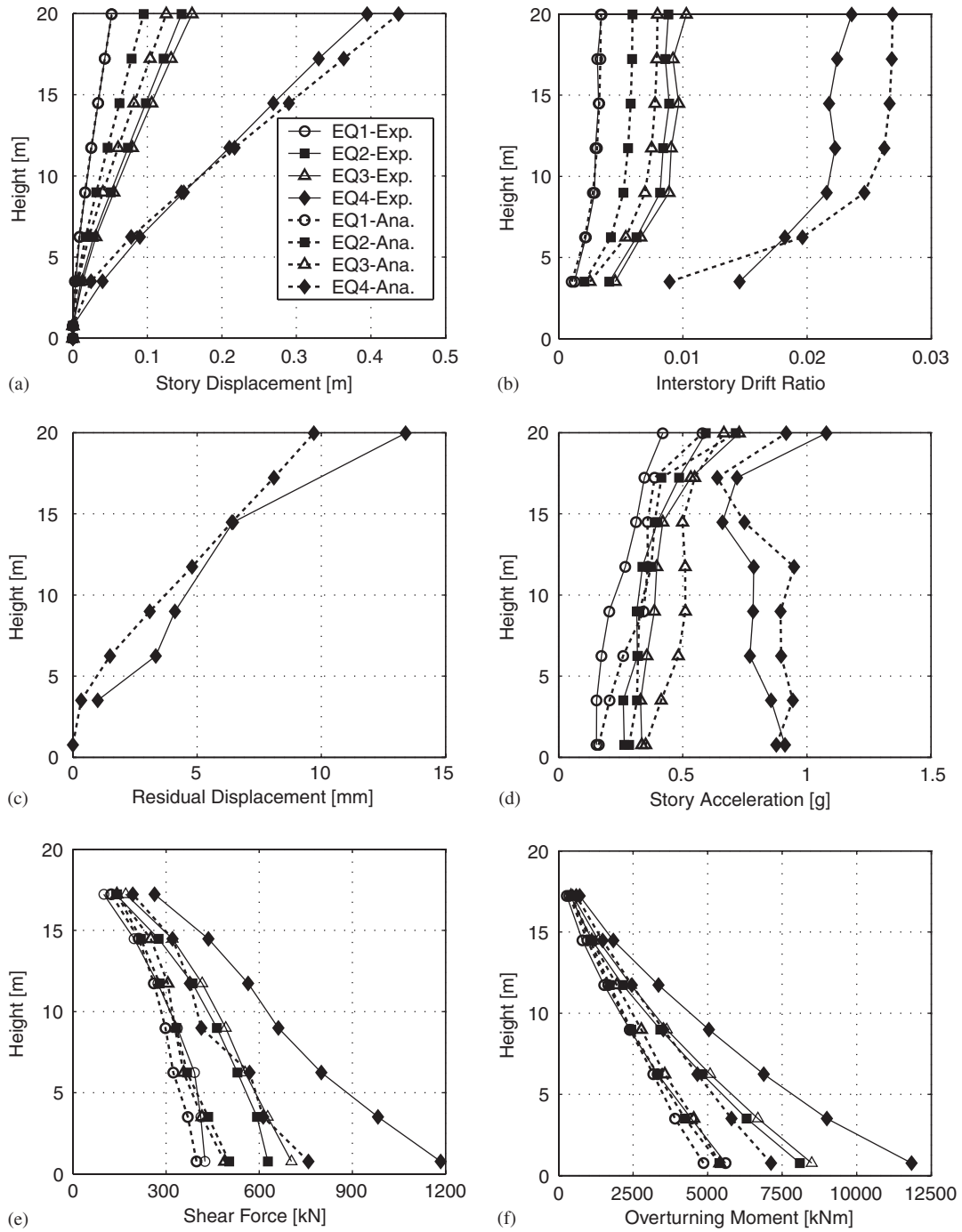


Figure 8. Experimental and analytical envelopes: (a) displacement; (b) interstory drift; (c) residual displacement; (d) floor acceleration; (e) shear force; and (f) overturning moment.



DOI: 10.1002/eqe

Table III. Maximum response values from time-history analysis and test measurements.

| | EQ1 | | | EQ2 | | | EQ3 | | | EQ4 | | |
|---|---|---|---|---|---|---|---|---|---|---|---|---|
| | Exp | Com | Err | Exp | Com | Err | Exp | Com | Err | Exp | Com | Err |
| $u_{top}$ (mm) | 52 | 52.3 | 0.6 | 146 | 95 | −34.9 | 160 | 126 | −21.3 | 395 | 437 | 10.6 |
| $drift_{top}$ [$\times 10^{-3}$] | 3.46 | 3.41 | −1.5 | 8.84 | 5.95 | −32.7 | 10.3 | 7.97 | −22.7 | 23.60 | 26.90 | 14.0 |
| $u_{top,res}$ (mm) | — | — | — | — | — | — | — | — | — | 13.40 | 9.70 | −27.6 |
| $a_{top}$ (g) | 0.42 | 0.58 | 38.1 | 0.59 | 0.71 | 20.3 | 0.73 | 0.67 | −8.2 | 1.08 | 0.92 | −14.8 |
| $V_{base}$ (kN) | 425 | 398 | −6.3 | 628 | 503 | −19.9 | 704 | 489 | −30.5 | 1185 | 759 | −35.9 |
| $M_{base}$ (kNm) | 5606 | 4859 | −13.3 | 8093 | 5391 | −33.4 | 8490 | 5410 | −36.3 | 11 839 | 7124 | −39.8 |

Table IV. Average error for the envelope of the maximum response value.

| | EQ1 | EQ2 | EQ3 | EQ4 |
|---|---|---|---|---|
| Average displacement error (%) | 5.0 | 38.2 | 27.5 | 12.3 |
| Average drift ratio error (%) | 5.7 | 35.7 | 22.6 | 19.2 |
| Average residual displacement error (%) | — | — | — | 34.8 |
| Average acceleration error (%) | 35.8 | 10.5 | 21.7 | 14.4 |
| Average shear force error (%) | 11.6 | 22.4 | 28.3 | 32.3 |
| Average overturning moment error (%) | 12.9 | 22.8 | 24.6 | 28.6 |

improved after the conclusion of the contest by including the effect of the shear connectors in the slab connecting the web and the flange wall on the axial force and overturning moment of the wall.

A more comprehensive yet a concise model accuracy indicator can be obtained from the envelope of maximum response values in Figure 8. This indicator $\bar{e}$ is defined as the mean of the normalized error between measured and predicted response values over all stories of the specimen

$$\bar{e} = \left( \sum_{i=1}^{N} \left| \frac{x^i_{com} - x^i_{mea}}{x^i_{mea}} \right| \right) \cdot \frac{1}{N} \cdot 100 \tag{1}$$

where $x^i_{com}$ and $x^i_{mea}$ denote the predicted and measured maximum value of response variable $x$ at the $i$th story, respectively, and $N$ is the number of stories. Table IV reports this average error $\bar{e}$ for the response variables of Figure 8 for each input motion.

In addition to the envelope values, the response time history for displacements and internal forces offers insight into the damage evolution of the structural model during the four input motions. Figures 9 and 10 compare the measured response with the analytical time history of the relative top displacement of the web shear wall, and with the overall system base shear for all the four input motions. The agreement between analysis and experiment is quite remarkable for all the four motions. Again, the analytical model underestimates the maximum measured base shear force



DOI: 10.1002/eqe

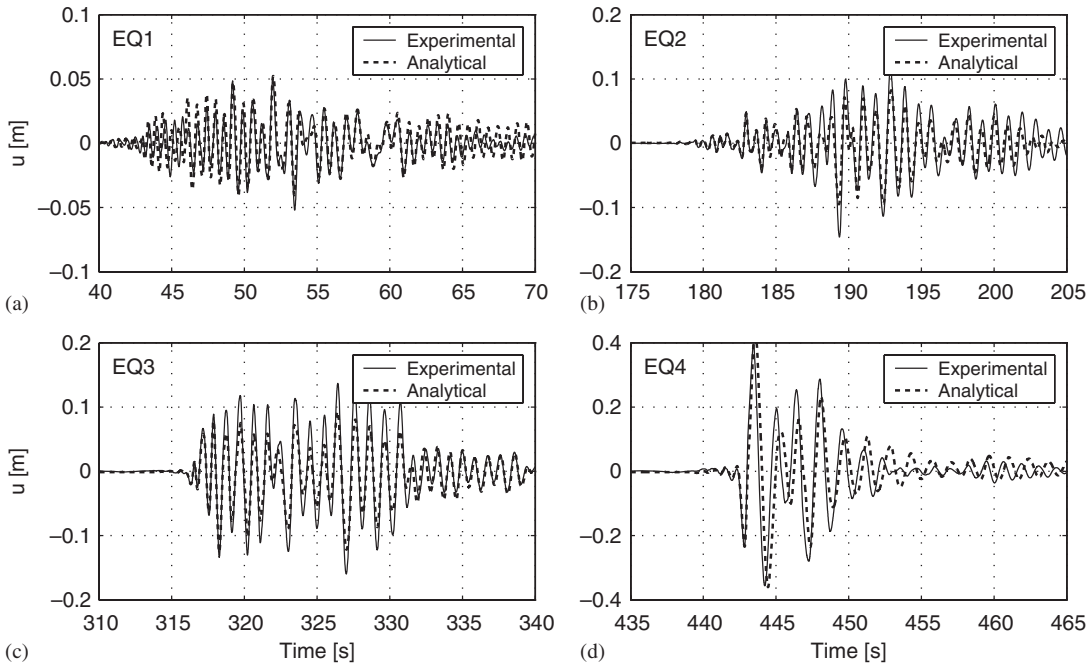


Figure 9. Comparison of experimental and analytical values for the top displacement during the four input motions.

value especially during the last input motion (Figure 10(d)). The agreement of the analytical with the experimental results for the last motion is especially noteworthy when one accounts for the damage accumulated during the previous input motions.

For a more accurate assessment of the capability of the proposed model to describe the damage evolution of the test specimen during the four input motions of increasing intensity, the frequency spectrum of the top displacement time history of the model is compared with the spectrum of the measured response. Figure 11 shows the frequency spectrum for a 6 s window at the beginning and at the end of each input motion. The spectrum at the beginning of each motion is represented with a thin line, while that at the end of each motion is represented with a thick line. Each frequency spectrum is normalized to the corresponding maximum value for the input motion. Since no difference in frequency between the end of EQ2 (EQ3) and the beginning of EQ3 (EQ4) was found, for the sake of clarity only the frequency at the end of EQ2 (EQ3) has been reported in Figure 11; this leads to six curves for each figure instead of eight. It is worth noting that the fundamental frequency of both the model and the test specimen changed from 1.9 Hz at the beginning of the first input motion to 0.67 Hz at the end of the last input motion. The corresponding fundamental period values were 0.52 s and 1.49 s, respectively. Thus, despite the significant lengthening of the fundamental period of the specimen by more than 2.5 times, the numerical model was able to track this damage evolution with remarkable accuracy. The comparison, in terms of acceleration Fourier spectra, between each base input motion and the corresponding motion at the top of the structure (both not reported here), confirms that the peaks in Figure 11 represent the damage evolution of the structure and are not influenced by the base input peaks.



DOI: 10.1002/eqe

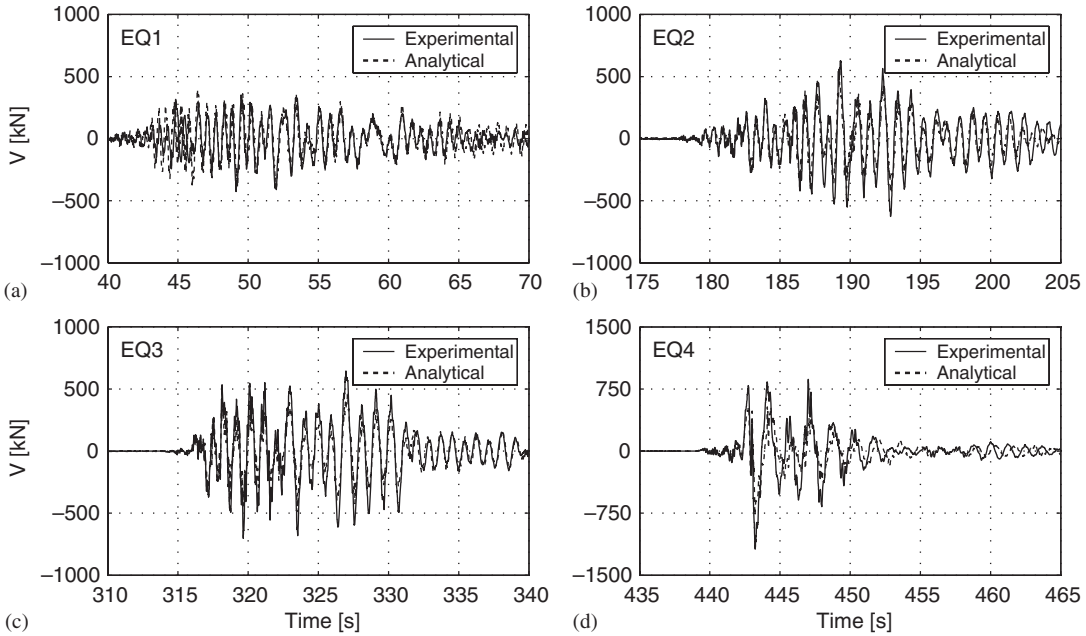


Figure 10. Comparison of experimental and analytical values for the shear force at wall base during the four input motions.

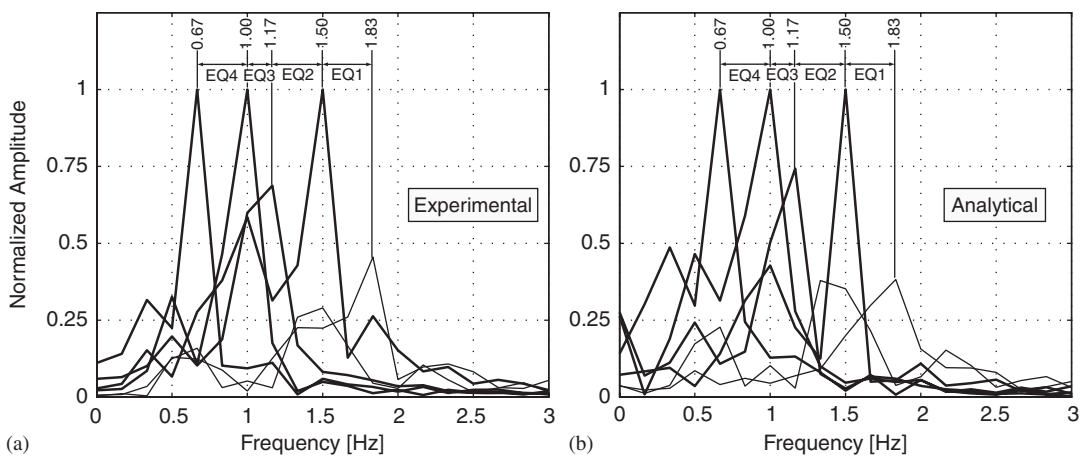


Figure 11. Evolution of frequency spectrum during the four input motions: (a) experimental and (b) analytical.

Another point of considerable interest in performance-based seismic evaluation is the determination of local damage in the concrete and in the reinforcing steel. Figure 12(a) shows the envelope of steel strains in an outer reinforcing layer along the height of the web wall. The agreement with



DOI: 10.1002/eqe

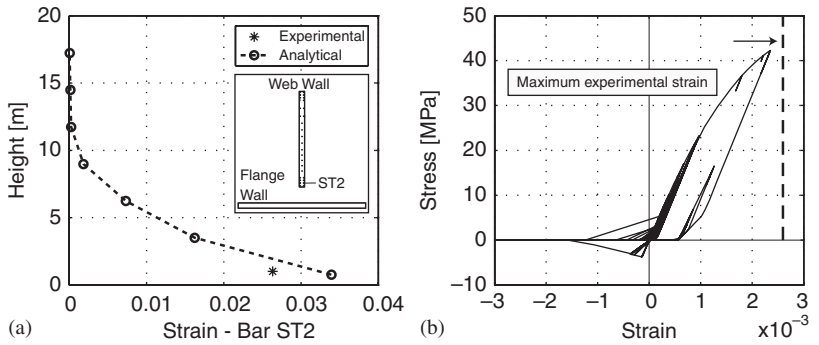


Figure 12. Local response for EQ4: (a) strain envelope for reinforcing bar ST2 and (b) stress–strain relation for concrete fiber at wall base level.

the single experimental value near the base of the wall is quite good. Figure 12(b) shows the hysteretic behavior of the outermost concrete fiber at the wall base. Again, the analytical value is in good agreement with the measured strain. The good agreement confirms the selection of only three integration points for each beam–column element of the shear-wall specimen model.

### *4.2. Post-test evaluation of the shear wall specimen*

The comparison of the blind predictions with the experimental results at the conclusion of the contest revealed an underestimation of internal forces in the web wall especially during the peak response of the strongest table motion. This underestimation arose despite the very good agreement in displacement and deformation time histories. From the careful study of the experimental results and the insight gained from the analytical results of other participants in the contest it was concluded that 3d aspects of the specimen response gave rise to additional axial forces in the web wall, thus altering its capacity. The 2d model does not take into account the additional forces generated by the deformation of the slab, and the slotted connectors between the web and the flange shear wall. The importance of such effects was relatively clear at the beginning of the blind contest, but the lack of time and resources for this undertaking did not allow the development of a 3d finite element model. Since the latter is relatively time and resource consuming, it was decided to assess the importance of some of these factors after the contest still within the framework of the original 2d model of the shear wall specimen. To this end an approximate way of representing the effect of the slotted connectors and of assessing its influence on the shear wall response was pursued, as will be described in the following.

In the analytical model for the blind contest the slotted connectors between the web wall and the flange wall were modeled with truss elements, thus ignoring any bending moments and the associated shear forces in the slotted connectors. The experimental results and the insight from the discussions with the experimental team led to the conclusion that this effect albeit small per unit length of the connector gave rise to an appreciable force when summed up over the length of the connection between flange and web wall.

The moment capacity of the slotted connector stems from the small dimension of its teeth (Figure 3). The maximum moment from a sectional analysis under the assumption that plane sections remain plane gives a value per unit length of the connector equal to $M_u = 10.45\,\mathrm{kNm/m}$



DOI: 10.1002/eqe

for the side connecting to the web wall, and $M'_u = 5.95$ kNm/m for the side connecting to the flange wall. When both sides of the slotted connector reach the moment capacity, the maximum shear force that can be transferred across the connector can be readily derived from equilibrium considerations and is equal to

$$V_{\max} = \frac{M_u + M'_u}{l} = \frac{10.45 + 5.95}{0.635} = 25.8\,\text{kN/m} \tag{2}$$

where $l$ is the distance between the edge of the web wall and the edge of the flange wall. Although the moment and shear force values are small per unit of length, they result in an appreciable force transfer when summed up over the entire length of the wall connection, which amounts to approximately 5 m (Figure 2). The presence of slotted connectors at each floor of the specimen thus results in a significant modification of the axial force in the web and the flange walls.

It is possible to introduce the moment transfer of the slotted connectors in the original model by modifying the truss element into a frame element. This would require including the interaction of the slotted connectors with the surrounding slab, which is not only supported by the shear walls but by the gravity columns as well. Thus, a complex 3d model would result. This would also entail a change in the vibration characteristics of the original model and necessitate the complete revision of the original results. Since time and resources were not available for such an extensive investigation, it was decided to introduce this effect with a shortcut, so as to estimate its importance before embarking on a more detailed investigation in a future opportunity. The shortcut consisted of determining the magnitude of the maximum shear force that can be transmitted by the connectors and applying it as an external force at the edge of the flange and web walls over the duration of maximum response. It was, thus, assumed that the connectors reach the moment capacity at both the ends during the maximum excursion of the shear wall into the inelastic range during EQ4. Under the assumption that the maximum deformation in the slotted connectors is in phase with the displacement response, and under the further assumption that the latter is governed by the first mode of vibration, it was decided to vary the applied forces as a sine function with period equal to the period of the first mode, as determined from the frequency response spectrum for EQ4 (Figure 11). This variable force was applied over an interval of 3 s duration centered at the acceleration peak of EQ4. The model of the shear wall specimen with this approximate consideration of the effect of the shear force transfer in the slotted connectors is referred to in the following as ‘SC model’.

The comparison between the results of the model used for the blind prediction contest, herein referred to as ‘Basic model’ and those of the ‘SC model’ is shown in Figure 13 in terms of the shear force and the overturning moment envelopes for the strongest motion EQ4. The significant effect of the slotted connectors is rather clear and leads to a notable improvement of the agreement of the ‘SC model’ with the experimental results. The base shear force and overturning moment error decreases from 35.9 to 13.8% and from 39.8 to 8.3%, respectively. To illustrate better the effect of the slotted connectors Figure 14 compares the time history of base shear force (Figure 14(a)) and base overturning moment (Figure 14(b)) of the two models with the experimental results. The comparison is limited to a time interval around the peak response of the specimen for EQ4. It is evident from these comparisons that the shear force of the slotted connectors gives rise to an additional axial force in the web wall that affects the moment capacity and, consequently, the wall shear force value (Figures 13(a) and 14(a)). This effect is more pronounced when the specimen is displaced westward, when the web wall experiences an additional compression force, while the flange wall compression force is reduced by the same amount.



DOI: 10.1002/eqe

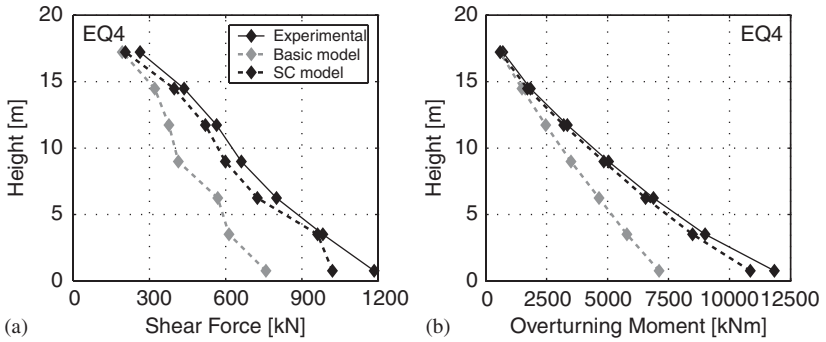


Figure 13. Comparison between the envelopes of the 'Basic' and the 'SC' model for EQ4: (a) story shear force and (b) story overturning moment.

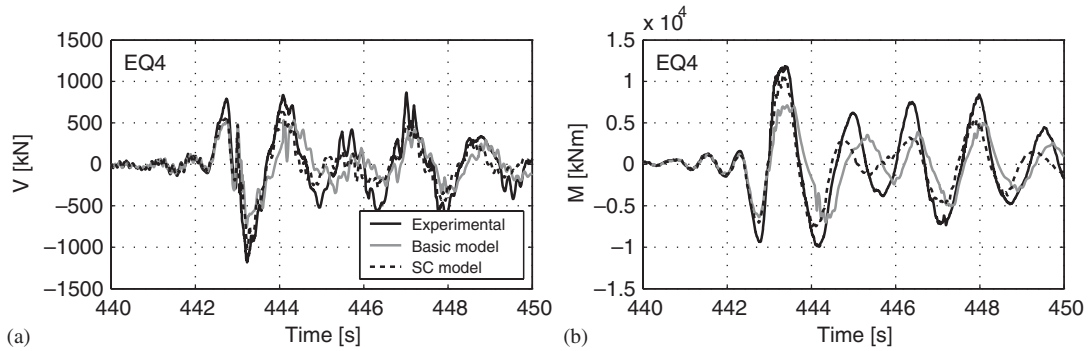


Figure 14. Comparison between the time histories of the 'Basic' and 'SC' model for EQ4: (a) base shear force and (b) base overturning moment.

In summary, the small moment capacity of the slotted connectors gives rise to three distinct contributions that affect the internal force distribution in the web and flange walls of the specimen: (a) a small bending moment that is directly transmitted to the web and flange walls, (b) a shear force that increases or decreases the axial compression in the web and flange walls due to gravity and thus increases or decreases the moment capacity of the wall, respectively, and (c) an additional overturning moment due to the eccentricity of the connector shear force relative to the middle of the web wall. By contrast, the inclusion of the slotted connector effect does not influence appreciably the story displacement and interstory drift values: the error for the maximum roof displacement of the shear wall during EQ4 increases from 10.7% for the 'Basic model' to 17.5% for the 'SC model'.

## 5. CONCLUSION

This paper describes the numerical model of a full-scale vertical slice of a seven-story R/C wall building and the simulations of its nonlinear response to shaking table excitations representing



DOI: 10.1002/eqe

earthquake ground motions. The shear wall building was subjected to four consecutive table motions with increasing maximum acceleration from 0.15 to 0.93$g$, representative of low, medium, and high levels of excitation. This excitation history caused increasing damage in the structure up to pronounced nonlinear hysteretic behavior and lap splice failure during the last input motion. Under the constraint of time and available resources for the participation in a blind prediction contest, the study adopted a 2d model for the specimen with one fiber beam–column element with three integration points for each story of the web and the flange walls.

For R/C walls of medium to high slenderness undergoing primarily flexural response with negligible shear effects, the Euler–Bernoulli fiber beam–column element with force formulation is a good compromise between accuracy and computational efficiency. The ability of the proposed model to predict the measured earthquake response of a R/C shear wall specimen was demonstrated by the good agreement of the blind prediction results with the measured data. This comparison covered the time histories of floor displacements and base shear force, and the envelopes of floor displacement, interstory drift, floor acceleration, story shear, and overturning moment over the height of the structure. The ability of the proposed model to track the damage evolution of the specimen was confirmed by the comparison of the frequency spectrum evolution during the four input motions. The maximum strain values of the model agreed well with isolated measurements of steel and concrete strains at the base of the wall. For such a good agreement of local response it is recommended to represent each structural member with a single element and to use three or four integration points for each beam–column element. It is noteworthy that a force-based element does not require mesh refinement for increased accuracy of inelastic response, as is the case with displacement-based formulations. The assumption of perfect bond between concrete and steel in the fiber beam–column element did not play an important role in the representation of the inelastic specimen response. The lack of a bond-slip model with pull-out capability, however, did not permit the model to capture the lap splice failure of the specimen during EQ4.

The comparison of the analytical results with the measured values after the conclusion of the blind contest brought to light the significant effect played by the shear transfer in the slotted slab connection between the web and flange walls. The internal forces modify the axial force in the web and flange wall and thus affect the moment capacity. Moreover, they directly affect the overturning moment of the web wall, since they act at the edge of the cross-section. An approximate estimation of this effect confirmed its importance in the determination of the internal forces of the specimen. It is, therefore, recommended that a more sophisticated 3d model of the slab–wall interaction be used in future studies.

The study presented herein reveals the potential of existing software in representing the hysteretic response of complex structural systems, but it also reveals the need for more sophisticated analyses and integrated experimental–analytical studies in order to develop a better understanding of the complex interplay between the different components of the specimen. The accuracy of the authors' model for the blind prediction contest is a warning that a good match with most of the measured data is no guarantee that the internal force distribution and the interplay of the specimen components has been fully captured by the model. Professional engineers are, therefore, strongly cautioned to use judgment in the interpretation of the inelastic dynamic response of a structure.

## ACKNOWLEDGEMENTS

The authors thank NEESinc, the Portland Cement Association, and the University of California at San Diego for funding the Blind Prediction contest. The first author is grateful to the Department of Structural



DOI: 10.1002/eqe

Engineering of the Politecnico di Milano for the financial support in the form of a doctoral fellowship for his stay at the Department of Civil and Environmental Engineering at the University of California, Berkeley. The first author is also grateful to Professor Maria G. Mulas for the fruitful discussion during the course of the study.

## REFERENCES

1. NEES7Story. *NEES@UCSD Seven-Story Building-Slice Earthquake Blind Prediction Contest*. Available from: http://nees.ucsd.edu/7Story.html [27 May 2008].
2. Panagiotou M, Restrepo JI, Conte JP, Englekirk RE. Seismic response of reinforced concrete wall buildings. *Proceedings of the 8th U.S. National Conference on Earthquake Engineering*, San Francisco, CA, U.S.A., 2006.
3. Panagiotou M, Restrepo JI, Englekirk RE. Experimental seismic response of a full scale reinforced concrete wall building. *First European Conference on Earthquake Engineering and Seismology*, Paper Number 201, Geneva, Switzerland, 2006.
4. Panagiotou M, Restrepo JI. Model calibration for the UCSD 7-story building slice. *NEES-UCSD Workshop*, *Analytical Model of Reinforced Concrete Walls*, San Diego, CA, U.S.A., 2006.
5. Englekirk RE. *Seismic Design of Reinforced and Precast Concrete Buildings*. Wiley, Inc.: Hoboken, NJ, 2003.
6. Priestley MJN, Kowalsky MJ. Direct displacement-based seismic design of concrete buildings. *Bulletin of the New Zealand National Society for Earthquake Engineering* 2000; **33**(4):421–444.
7. McKenna F, Fenves GL, Scott MH. *Open System for Earthquake Engineering Simulation*, University of California, Berkeley, CA, 2000. Available from: http://opensees.berkeley.edu [27 May 2008].
8. Scott MH, Fenves GL. Plastic hinge integration methods for force-based beam-column elements. *ASCE Journal of Structural Engineering* 2006; **132**(2):244–252.
9. Zienkiewicz OC, Taylor RL, Zhu JZ. *The Finite Element Method*: *Its Basis and Fundamentals* (6th edn), vol. I. Elsevier, Butterworth-Heinemann: Amsterdam, 2005.
10. Spacone E, Filippou FC, Taucer FF. Fibre beam–column model for nonlinear analysis of r/c frames: Part I, formulation. *Earthquake Engineering and Structural Dynamics* 1996; **25**(7):711–725.
11. Filippou FC, Fenves GL. Methods of analysis for earthquake-resistant structures. In *Earthquake Engineering*: *From Engineering Seismology to Performance-based Engineering*, Chapter 6, Bozorgnia Y, Bertero VV (eds). CRC: Boca Raton, FL, 2004; 6.1–6.65.
12. Kent DC, Park R. Flexural member with confined concrete. *Journal of Structural Division*, *Proceedings of the American Society of Civil Engineers* 1971; **97**(ST7):1969–1990.
13. Park R, Priestley MJN, Gill WD. Ductility of square-confined concrete columns. *ASCE Journal of the Structural Engineering* 1982; **108**(4):929–950.
14. Scott BD, Park R, Priestley MJN. Stress–strain behavior of concrete confined by overlapping hoops at low and high strain rates. *ACI Journal Proceedings* 1982; **79**(1):13–27.
15. Menegotto M, Pinto P. Methods of analysis for cyclically loaded R/C frames. *Proceedings of the Symposium of Resistance and Ultimate Deformability of Structure Acted by Well Defined Repeated Load*, IABSE, Lisbon, Portugal, 1973.
16. Filippou FC, Popov EP, Bertero VV. Effects of bond deterioration on hysteretic behavior of reinforced concrete joints. *Technical Report EERC-83/19*, Earthquake Engineering Research Center, University of California, Berkeley, 1983.
17. Moaveni B, He X, Conte JP, Restrepo JI. System identification of a seven-story reinforced concrete shear wall building slice tested on the UCSD-NEES shake table. *NEES-UCSD Workshop*, *Analytical Model of Reinforced Concrete Walls*, San Diego, CA, U.S.A., 2006.
18. Restrepo JI. *NEES-UCSD Workshop*, *Analytical Model of Reinforced Concrete Walls*, San Diego, CA, U.S.A., 2006.
19. Wilson EL. *Static and Dynamic Analysis of Structures*, *a Physical Approach with Emphasis on Earthquake Engineering*. Computers and Structures, Inc.: Berkeley, CA, 2000.



DOI: 10.1002/eqe